15TH IEA HEAT PUMP CONFERENCE
MAY 26–29, 2026 | HOFBURG
VIENNA 2026
DECARBONISATION THROUGH INNOVATION

Theoretical and experimental study on a frost-free refrigerated display cabinet

Li ZHANG[a,*], Komei NAKAJIMA[b,*], Yusuke TASHIRO[b], Hikaru YAMADA[a],

Tomohiro HIGASHI[a]

[a]Central Research Institute of Electric Power Industry, 2-6-1 Nagasaka, Yokosuka, Kanagawa Prefecture, 240-0196, Japan
[b]Mitsubishi Electric Corporation, 3-18-1, Oshika, Suruka Ward, Shizuoka Prefecture, 422-8528, Japan

Abstract

Frosting is a common phenomenon in refrigerated display cabinets (RDCs). As the frost layer thickens, the heat transfer rate and airflow through the evaporator dramatically decline, thus reducing cooling efficiency and increasing energy consumption. Defrosting of RDC evaporators can be achieved using several methods, including off-cycle defrost, electric defrost, hot-gas defrost, and reverse-cycle defrost. However, these methods may lead to several issues such as temperature fluctuations within the cabinets, increased energy consumption, water pooling, and bacterial growth in the drain pan. In this study, a desiccant is applied to eliminate moisture from the air entering the evaporator, thereby preventing frost formation. We propose a frost-free RDC that mainly comprises a compressor, two desiccant-coated heat exchangers (DCHEs), a low-temperature evaporator and an auxiliary condenser. The return air of the RDC is dehumidified due to one of the DCHEs to prevent the evaporator frosting. Meanwhile, another DCHE works as a condenser, in which the desiccant is regenerated using condensation heat that would otherwise be ejected into the ambient air in conventional RDCs.

A theoretical and experimental study is conducted for a forced draft, open-type frost-free RDC, with a cabin volume of 67L and a cabin temperature of 2~8°C. Simulation results show that the required air cooling load of the RDC is 0.43kW and the electric power consumption of the compressor is 0.14kW, respectively. A prototype of the frost-free RDC was made and experiments were conducted. The experimental results show that eliminating defrost cycles in the prototype helps stabilize the internal cabin temperature. Moreover, the proposed frost-free RDC has an energy saving potential of 35.7% compared to commercial RDCs.

Keywords: refrigerated display cabinet; frost-free; desiccant-coated heat exchanger; adsorption; dehumidification

1. Introduction

The demand for refrigerated and frozen foods is rising daily because of the recent population growth. In supermarkets and retail food stores, refrigerated display cabinets (RDCs), the last and vital link in the food chain between source and end users, are used to showcase the product on sale and maintain food temperature. For obvious reasons, moist air becomes entrained within the RDCs. Since the temperatures of the evaporators within the RDCs are lower than the dew point of the entrained air, water vapor within the air will condense and freeze on the evaporator surfaces, forming frost. As it thickens, the heat transfer rate and airflow through the evaporator dramatically decline, thus reducing cooling efficiency and increasing energy consumption [1-

* Corresponding author. Tel.: +81-46-856-2121
Email address: zhangli@criepi.denken.or.jp
* Corresponding author. Tel.: +81-54-287-3053
Email address: Nakajima.Komei@bc.MitsubishiElectric.co.jp

4]. Therefore, the accumulated frost should be removed from the evaporator coils periodically before it noticeably degrades their performance.

Defrosting of the evaporators of RDCs can be achieved by several methods: off-cycle, electric heating, hot-gas and reverse-cycle defrost method. For the off-cycle defrost method, the refrigerant compressor is turned off and the frost melts naturally utilizing the air inside the RDC. This method is suitable for medium- to high-temperature display cabinets. Due to the limited heat from the air, defrosting takes far longer than other defrosting methods [5]. The electric heating defrost method, in which electric resistance heaters are installed on the evaporator coils to melt frost, can remove frost quickly and effectively and is widely used in commercial RDCs. For the hot-gas defrost and reverse-cycle defrost methods, the high-temperature refrigerant from a compressor is directly channeled to the evaporators instead of flowing into a condenser and provides the required heating to melt the frost. Although the two defrost methods are considered to have an higher defrosting efficiency and shorter defrosting time theoretically, they have not been commercially applied to RDCs to date, due to the complex piping and system design required [6].

Those existing defrost methods may lead to several issues:

- ✓ Temperature fluctuations inside the cabin
- ✓ Increased energy consumption
- ✓ Water pooling and bacterial growth in the drain pan

The temperature fluctuations during the defrost process were found to exceed 12°C in the electric heater defrost method [5], [7], [8]. The temporary rise in temperature inside the RDCs affects food safety and product quality, at worst may damage food. Some efforts have been made to reduce the temperature fluctuations during defrosting. [9] and [10] proposed a composite shelf designed for the vertical open RDC, which is based on heat pipe technology and the cool storage characteristics of phase change materials among the heat pipes. The temperature fluctuation of food packages was reduced by 53.3–83.3% during defrosting [9]. The food temperature in the new shelf was reduced by 1.5 °C during defrosting period [10]. [7] proposed a new defrost method, which utilizes the heat from the liquid refrigerant to defrost the evaporator using two evaporators and a four-way valve. The temperature fluctuation is about 4.5 °C in the new defrost method.

Electric defrosting significantly increases energy usage and impacts operational costs. [11] indicated that only 15 to 20% of the heat supplied for defrosting was actually carried out by the condensate. [12] reported that electric defrost heaters can account for up to 25% of the total electrical energy consumption of refrigerated display cases. [5] reported that while the efficiency of a defrost heater was 30.3 %, the power consumption of the freezer increased by 17.7 % due to automatic defrosting. A review of manufacturers' data indicates that electric defrost energy consumption can range from 10 to 30% of the total display case energy consumption, with an average of approximately 20% [13]. Furthermore, defrosting adds heat to the refrigerated display cases, which must then be removed by the refrigeration system after the defrost cycle is terminated, thereby increasing compressor operation and energy use.

For any of the defrost methods mentioned above, proper drainage systems are required to prevent water pooling. In common, the defrosted water traverses a tube, is collected in a tray pan, which is often located close to the compressor or condenser and finally evaporates from the tray pan due to the heat of the compressor or condenser. This system works satisfactorily in countries where the ambient air has low relative humidity and the amount of defrosted water is limited. However, under hot and humid ambient conditions, more defrosted water is generated, but at a slower evaporation speed, which may lead to water overflowing from the tray pan [14]. In addition, electrical resistance in a tray pan is activated as required, accelerating the removal of defrost water by evaporation. Using a heater can reduce the drying time, but increases energy consumption [15].

Most of the previous studies focused on how to remove frost quicky and efficiently. In other words, frosting on evaporator surface is initially allowed. In our study, a desiccant is applied to eliminate moisture from the air entering the evaporator, thereby preventing frost formation and eliminating defrost process. Desiccants are well-known as efficient means of air dehumidification. Some researchers have proposed a method to prevent air-source heat pumps from frosting, i.e. in which air is dehumidified by a solid adsorbent before entering the evaporator [16]-[20].

We found almost no reports about preventing frost with desiccant in RDCs. In this study, the idea of using desiccant to prevent an air-source heat pump frosting is applied to develop a frost-free refrigerated display cabinet (frost-free RDC). A theoretical and experimental study is conducted on the novel frost-free RDC. The configuration and principle of the frost-free RDC is described, and the simulation and experimental results are given.

2. System description

A schematic diagram of the proposed frost-free RDC is shown in Fig. 1, with the process illustrated on a pressure-enthalpy diagram of the refrigerant and a psychometric chart in Figs. 2 and 3. The system comprises a compressor, an evaporator, a condenser, two desiccant-coated heat exchangers (DCHE_1 and DCHE_2), two expansion valves (V1 and V2) and a four-way valve. DCHE is a unique heat exchanger, in which the surface of the fins and some of the tube surfaces are coated with desiccant and has moisture adsorption ability. Compared with a conventional RDC, this system can dehumidify the return air (RA) before it enters the evaporator, thereby preventing frost from forming. The moisture-adsorbing capacity of the DCHE will decrease and eventually expire as the adsorption process progresses, so it should be periodically regenerated (desorbed). In this proposed system, to prevent the evaporator frosting on an ongoing basis, two DCHEs are applied: When one operates under the adsorption (AD) process to absorb moisture from the return air, another is regenerated under the desorption (DE) process and the AD/DE processes are switched periodically. Here, when DCHE_1 operates under the AD and DCHE_2 under the DE processes, we name them Mode A; DCHE_1 under the DE and DCHE_2 under the AD process, named Mode B.

During Mode A, the refrigerant exiting the compressor at the state of "1" flows into the condenser, in which it releases one part of condensation heat to the outside air (OA2). After leaving the condenser, the refrigerant flows through the four-way valve and into the DCHE_2, in which it releases the remaining condensation heat to the desiccant. Consequently, the desiccant is regenerated and the OA1 after absorbing the moisture and heat is exhausted (EA1). The refrigerant at the state of "3" leaving the DCHE_2 is expanded to intermediate pressure by flowing through the expansion valve 1 (V1) and flows into the DCHE_1, while the return air (RA) from the display cabinet is dehumidified at the DCHE_1 due to the AD process. The adsorption heat of the desiccant is used to vaporize one part of the refrigerant to the state of "5", whereupon the refrigerant "5" is expanded to the required evaporation pressure (P_{low}) by traversing another expansion valve 2 (V2) and flows into the evaporator. Within the evaporator, the refrigerant is vaporized and the dehumidified air (DA) exiting the DCHE_1 is cooled and leaves in the state of the supply air (SA), which is supplied to the display cabinet. Because the dew point of the DA is lower than the surface temperature of the evaporator, a frost-free state can be realized at the evaporator. When the water content of the desiccant in DCHE_1 becomes relatively high and the dehumidification capacity declines so that the dew point of the DA exceeds the evaporator's surface temperature, the system is switched to Mode B.

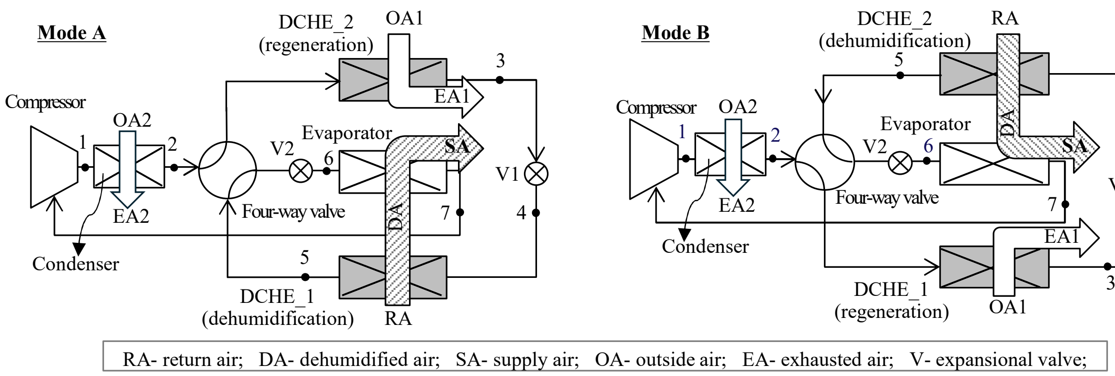

Figure 1 Schematic diagram of the frost-free RDC

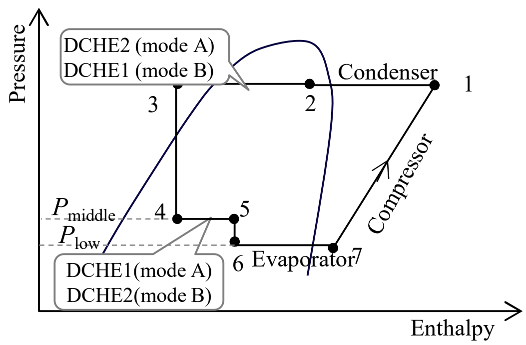

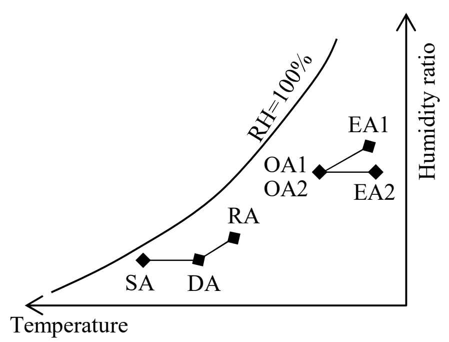

Figure 2 Pressure-enthalpy of refrigerant during both modes Figure 3 Psychometric chart of air during both modes

When the system operates under Mode B, the four-way valve works, so the refrigerant cycles in this order: Compressor → Condense → DCHE_1 → V1 → DCHE_2 → V2 → Evaporator → Compressor. The air flows of OA1 and RA are switched: OA1 → DCHE_1 and RA → DCHE_2. Regardless of the operation modes, the refrigerant and air undergo the same state change as shown in Figs. 2 and 3, separately.

3. Theoretical and experimental analysis of heat and mass-transfer characteristics in DCHE

The performance of the proposed frost-free RDC strongly depends on the heat and mass-transfer characteristics of the DCHEs. In this study, we developed heat and mass-transfer models and validated them by comparing the predictions with the experimental results.

3.1. Heat and mass-transfer models

Three DCHEs of equivalent size but with different polymer [21] coating amounts were adopted. The paragraphs and physical characteristics of these DCHEs are shown in Fig. 4 and Table 1, separately. The adsorption isotherm of the polymer is given in Fig. 5.

A schematic of the heat and mass transfer for the DCHE is shown on Fig. 6. Air flows through the DCHE and contacts the desiccant felt to exchange moisture (M_V), while brine inside the tubes is used to heat or cool the desiccant and the heat transfer rate between the brine and the air is q.

Before establishing heat and mass-transfer models, some assumptions were made as follows. The DCHE is considered a block, through which the air and brine flow at the desiccant-coated fin side and inside the tube separately. The desiccant material is evenly coated at the DCHE surface. The adsorption heat is assumed to be released to the desiccant layer only. However, it is transferred to the air and brine due to temperature difference.

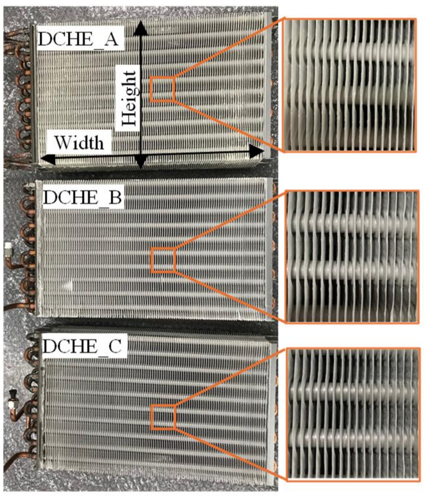

Figure 4 Paragraphs of three DCHEs

Table 1 Physical characteristics of DCHEs

Parameters	Value
Height (m)	0.22
Width (m)	0.35
Length in air flow direction (m)	0.076
Outer diameter of tube (m)	9.525×10^{-3}
Thickness of tube (m)	0.8×10^{-3}
Fin pitch (m)	3.5×10^{-3}
Thickness of fin (m)	0.3×10^{-3}
Desiccant material	Polymer (EXLAN)
Polymer coating amounts (kg) *Binder is excluded	DCHE_A: 0.26
	DCHE_B: 0.15
	DCHE_C: 0.064

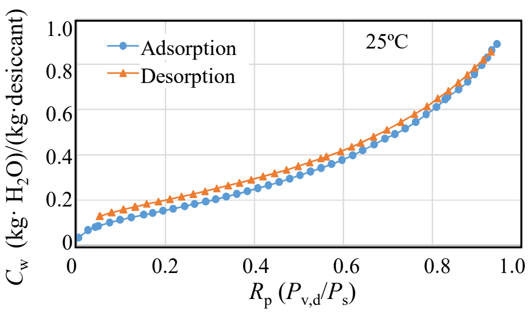

Figure 5 Adsorption isotherm of polymer

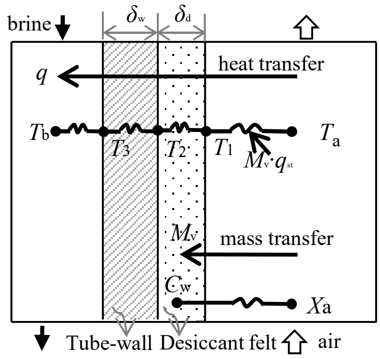

Figure 6 Schematic diagram of heat and mass-transfer

The mass-transfer rate (M_v) is calculated by Eq. (1).

$$M_v / M_{ve} = 1 - e^{-\emptyset\tau} \quad (1)$$

Here, M_{ve} - equilibrium mass-transfer rate [kg/s]; τ-time step [s]; φ- adsorption time constant [-], mainly affected by the desiccant coating amount per unit surface (S_d, [g/m^2]), the velocity of air (V_a, [m/s]) and the temperature of desiccant (T_d, [°C]). φ is obtained from experimental measurements and the empirical correlations of φ are given in Eqs. (2-a) and (2-b).

$$\varphi = 85\frac{1}{s_d}\cdot(0.0007V_a + 0.0003)\cdot e^{0.0696T_d} \quad V_a \leq 1 \text{ m/s} \quad (2\text{-a})$$

$$\varphi = 85\frac{1}{s_d}\cdot(0.001)\cdot e^{0.0696T_d} \quad V_a > 1 \text{m/s} \quad (2\text{-b})$$

The heat transfer between the air and brine comprises four processes: the heat transfer between the air and desiccant felt composed of one convective heat transfer (the first term on the right-hand side of Eq. (3)) and one latent heat transfer (the second term on the right-hand side of Eq. (3)), the heat conductions inside the desiccant felt and tube wall (Eq. (4), Eq.(5)), the convective heat transfer between the tube wall and the brine (Eq. (6).

$$q = h_{out}\cdot A_{out}\cdot(T_a - T_1) + M_v\cdot q_{st} \quad (3)$$

$$q = \frac{\lambda_d A_d}{\delta_d}(T_1 - T_2) \quad (4)$$

$$q = \frac{\lambda_w A_w}{\delta_w}(T_2 - T_3) \quad (5)$$

$$q = h_{in}\cdot A_{in}(T_3 - T_b) \quad (6)$$

From Eqs. (3) – (6), q can be rewritten in the form:

$$q = H_{total}\cdot A_{out}\cdot(\Delta T) + \frac{H_{total}}{h_{out}}M_v\cdot q_{st} \quad (7)$$

where H_{total} is the overall sensible heat transfer coefficient, expressed by Eq. (8). ΔT is the logarithmic mean temperature difference, calculate Eq. (9).

$$\frac{1}{H_{total}} = \frac{1}{h_{out}} + \frac{1}{h_{in}}\frac{A_{out}}{A_{in}} + \frac{\delta_d}{\lambda_d}\frac{A_{out}}{A_d} + \frac{\delta_w}{\lambda_w}\frac{A_{out}}{A_w} \quad (8)$$

$$\Delta T = \frac{(T_{b,in} - T_{a,out}) - (T_{b,out} - T_{a,in})}{ln\frac{T_{b,in} - T_{a,out}}{T_{b,out} - T_{a,in}}} \quad (9)$$

In this study, the conduction thermal resistances in the desiccant layer and tube wall are ignored, therefore, H_{total} is calculated by the Eq.(10). The inside and outside heat transfer coefficients (h_{in} and h_{out}) are calculated by Eqs. (11) and (12) separately [22], [23].

$$\frac{1}{H_{total}} = \frac{1}{h_{out}} + \frac{1}{h_{in}}\frac{A_{out}}{A_{in}} \quad (10)$$

$$N_{u,out} = \frac{h_{out}D_{ec}}{\lambda_a} = 2.1\left(\frac{Re,a\cdot Pr,a\cdot D_{ec}}{L}\right)^{0.38} \quad (11)$$

$$N_{u,in} = \frac{h_{in}D_{in}}{\lambda_b} = 0.023{R_{e,b}}^{0.8}{P_{r,b}}^{n} \quad (12)$$

n is 0.3 and 0.4 during the cooling and heating processes respectively.

3.2. Experimental measurements

Figure 7 shows a schematic diagram and photograph of the experimental apparatus. It comprises two air loops, two brine loops and some measurement instruments. During the adsorption (AD) experiment, the air at 12°C, 60% relative humidity and a velocity of 0.5 m/s from the air supplier_A and the cooling brine at 5°C and 5 liters per minute from the thermostatic bath_A are sent to the DCHE_A. During the desorption (DE) experiment, the air at 27°C, 60% relative humidity, and a velocity of 1m/s from the air supplier_B and the hot brine at 43°C and 5 liters per minute from the thermostatic bath_B are sent to the DCHE_A. AD and DE experiments were continuously conducted with at least three cycles per test, and the experimental data on the second or third cycle were used in the following data reduction. The temperature (T_a) and air humidity ratio (X_a) at the DCHE_A inlet and outlet are measured by P_t temperature sensors (accuracy to within±0.2 K), and a capacitive humidity sensor (accuracy to within ±1%). The air flow rate (m_a) is measured by a differential pressure flow meter (accuracy to within ±1.5%). The flow rates of the hot or cooling brine (m_b) at the DCHE_A inlet were measured by an electromagnetic flow meter (accuracy to within ±0.5% of the measured value). The brine temperature (T_b) was also measured at the DCHE inlet and outlet by P_t temperature sensors (accuracy to within ±0.2 K).

The mass-transfer rate of M_v is obtained from the measured results of m_a and X_a (Eq. (3)) The heat transfer rate of q is obtained from the measured results of m_b and T_b (Eq. (14)). M_v and q are also calculated by the proposed heat and mass-transfer models in Section 3.1. Both the experimental and calculated results of M_v and q are shown on Fig. 8. It is found that the values obtained by calculation correlate well with the experimental results.

$$M_v = m_a\left|X_{a,in} - X_{a,out}\right| \quad (13)$$

$$q = m_b C_{p,b}\left|T_{b,in} - T_{b,out}\right| \quad (14)$$

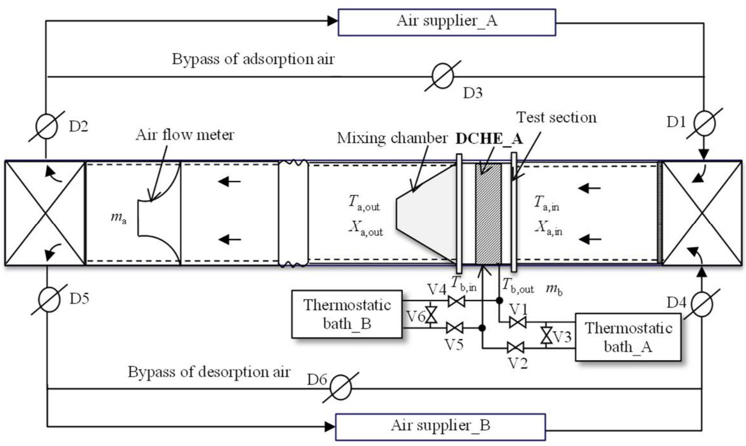

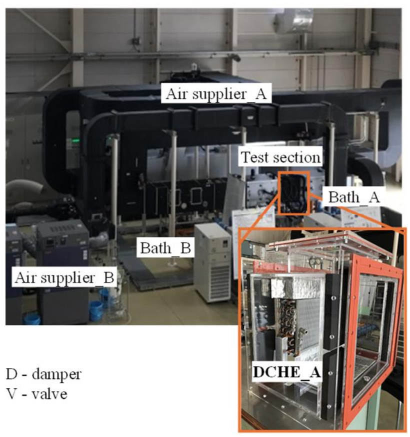

Figure 7 The schematic and photo of the experimental apparatus

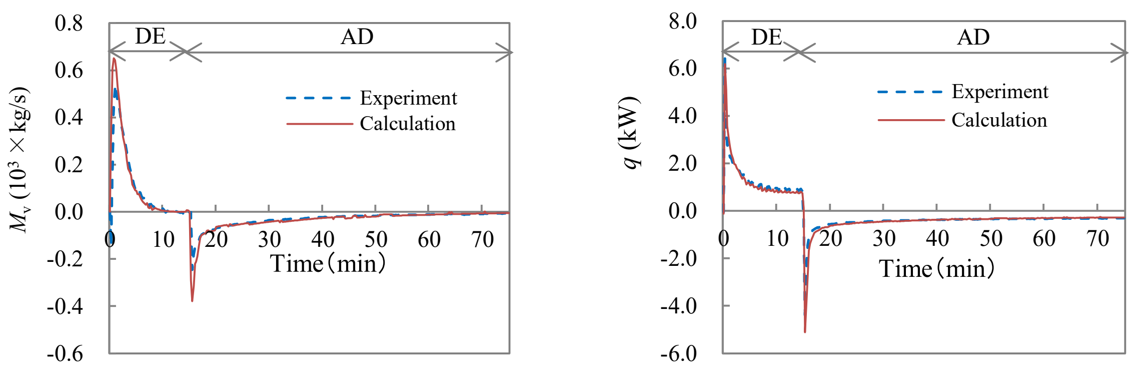

Figure 8 Comparison of experimental and calculated M_v and q

4. Simulation and experimental analysis of the proposed frost-free RDC

4.1. Simulation analysis

4.1.1. Calculation models

Simulations were carried out under the operating conditions shown in Table 2. The physical characteristics of the two DCHEs (DCHE_1 and DCHE_2) and the evaporator are shown in Table 3. In this simulation, the specifications of the condenser were not specified. We assumed that it could release the remained condensation heat of the refrigerant to maintain a constant supercooling (SC) of 2°C. As mentioned above, although the system switches between Modes A and B periodically, the refrigerant and air undergo the same state change. Accordingly, the mathematic models for either of the two modes can be applied to the other. In the following, the mathematical models based on Mode A will be established. During Mode A, DCHE_1 works as one of the two evaporators and the desiccant operates under the AD process, DCHE_2 as one of the two condensers under DE processes respectively.

The evaporation load of DCHE_1 (q_{eva1}) and condensation load of DCHE_2 (q_{con1}) are calculated by using the heat and mass-transfer models given in Section 3.1. The evaporation load of another evaporator (q_{eva2}) is calculated by Eq. (15). Therefore, the total evaporation load (q_{eva}) is obtained by Eq. (16). The mass flow rate of the refrigerant (m_r) is decided based on q_{eva}. The electric power consumption of the compressor (w_{com}) is calculated by Eq. (17). The remaining condensation load released by the condenser (q_{con2}) is calculated by Eq. (18).

$$q_{eva2} = H_{total,eva2} \cdot A_{out,eva2} \cdot \Delta T \quad (15)$$

$$q_{eva} = q_{eva1} + q_{eva2} \quad (16)$$

$$w_{com} = m_r(i_1 - i_7) \quad (17)$$

$$q_{con2} = q_{eva1} + q_{eva2} + w_{com} - q_{con1} \quad (18)$$

The switching time from Mode A to Mode B is decided by this relationship: namely, whether the dew point of the dehumidified air (DP_{DA}) is lower than the surface temperature of the evaporator (T_{sur}). T_{sur} is obtained by Eq. (19). If $DP_{DA}<T_{sur}$, then Mode A is continued. When this relationship can no longer be satisfied, Mode A ends and Mode B commences. DP_{DA} is a function of the humidity ratio of the dry air (X_{DA}) as calculated by Eq. (20).

$$h_{out,eva2}A_{out,eva2}\left(\frac{T_{a,in,eva2}+T_{a,out,eva2}}{2} - T_{sur}\right) = q_{eva2} \quad (19)$$

$$X_{DA} = X_{RA} - \frac{M_v}{m_{RA}} \quad (20)$$

Table 2 Parameters of the analytical calculation

Parameters	m_{RA}	T_{RA}	RH_{RA}	T_{SA}	m_{OA1}	T_{OA1}	RH_{OA1}	SC	SH	η_{com}
Values	0.015kg/s[1]	12ºC	70%	-5ºC	0.014kg/s	25ºC	60%	2ºC	5ºC	0.65

Note: m – mass flow rate; T-temperature; RH – relative humidity of air; SC – supercooling; SH – superheating; η_{com} – adiabatic efficiency of compressor; RA – return air; SA -supply air; OA – outside air.

Table 3 Physical characteristics of DCHEs and evaporator

Parameters	DCHE_1 and DCHE_2	Evaporator
Type of heat exchangers	Aluminum fin and copper tube	
Height×Width×Length (m)	0.254×0.252×0.0573	0.127×0.669×0.066
Fin pitch (m)	3.6×10^{-3}	1.8×10^{-3}
Surface area A_{out} (m^2)	1.99	5.63
Heat transfer coefficient (kW/(m^2·K)	0.017 of h_{out}; 0.016 of H_{total}	0.019 of h_{out}; 0.017 of H_{total}
Coated desiccant amount m_d (kg)	0.17	

Propane is used as a working fluid in this system, the thermophysical properties of which were calculated using REFPROP7.0 (NIST). The assumptions used in this simulation are as follows:

- ✓ Heat losses in the system are neglected.
- ✓ Constant isentropic efficiency of the compressor is assumed.
- ✓ A thermodynamic equilibrium exists between the air and desiccant in the desiccant-coated heat exchanger.
- ✓ The heat capacity change of the two DCHEs caused by the switch of adsorption/desorption processes is neglected.

4.1.2. Simulation results

The humidity ratio of air (X_a) at the DCHE_1 inlet and outlet is shown on Fig. 9. During Mode A, the return air (RA) with a humidity ratio of 6.2g/kg is dehumidified by the DCHE_1, therefore the outlet X_a is lower than that at the DCHE1 inlet. The outlet X_a rises over time and when it is equal to 3.63g/kg, the anti-frosting criteria can't be guaranteed, the operation mode is switched from A to B. During Mode B, the DCHE_1 is regenerated using the outside air (OA) with a humidity ratio of 12.7g/kg. The outlet X_a is higher than that at the DCHE_1 inlet.

The temperature of the return air (RA), the dehumidified air (DA) and the supply air (SA) is shown on Fig. 10. RA with a temperature of 12ºC is cooled to a temperature of 8ºC (DA) by the DCHE under AD process, and furthermore to -5ºC (SA) by the evaporator.

The total evaporation load (q_{eva}) and the electric power consumption of the compressor (w_{com}) are calculated, and the results are shown in Fig. 11. Both decrease slightly over time. The average values of q_{eva} and w_{com} for one cycle are 0.43kW and 0.14kW, respectively (Fig. 12). For 0.43kW of $q_{eva,ave}$, it consists of 0.28kW of the sensible heat load and 0.15kW of the latent heat load. The average moisture removed velocity over one cycle is 0.21kg/hour.

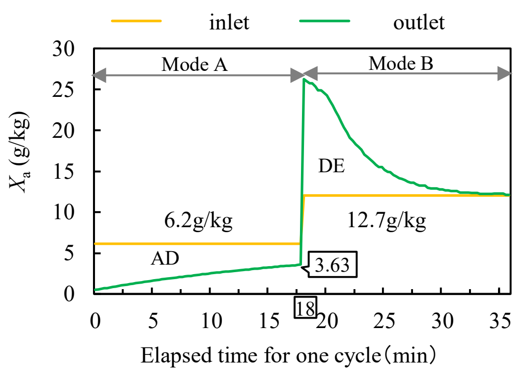

Figure 9 X_a at the DCHE_1 inlet and outlet

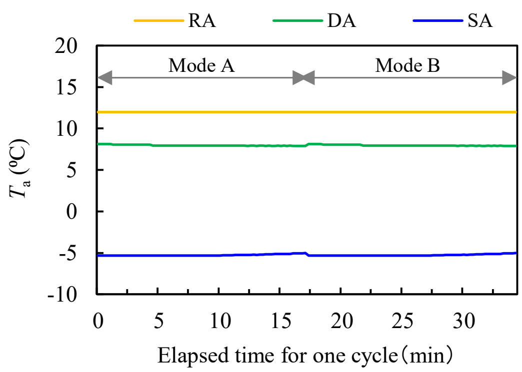

Figure 10 T_a of RA, DA and SA

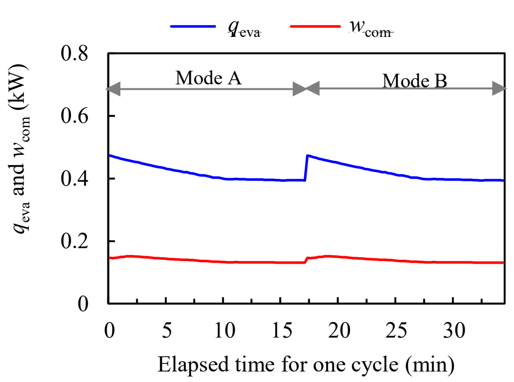

Figure 11 q_{eva} and w_{com}

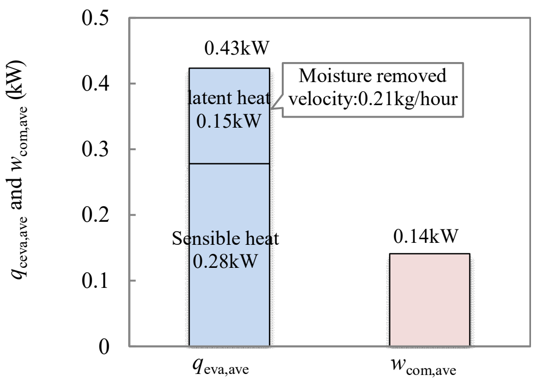

Figure 12 Average values of q_{eva} and w_{com}

4.2. Experimental analysis

We made a prototype: a forced draft, open-type frost-free RDC, with a cabin volume of 67 liters and cabin temperature of 2~8°C. As shown in Fig. 13, the prototype comprises a display cabin unit that is a commercially available conventional RDC and a DCHE unit, and the two units are connected by some refrigerant tubes and air ducts. The two DCHEs (DCHE_1 and DCHE_2) have the same specifications as those adopted in simulation analysis. However, the evaporator used in the prototype has greater overall dimensions and a larger fin pitch compared to that used in simulation analysis.

The prototype was installed in an environmental test chamber, within which the air was set to 26°C and relative humidity to 50%. Experiments were continuously conducted with at least two cycles per test. The refrigerant temperature and pressure at the inlet and outlet of the DCHE_1, DCHE_2, evaporator, condenser and compressor, the electric power consumption of the compressor, the air temperature and humidity ratio at the inlet and outlet of the DCHE_1, the evaporator are measured.

The measured results of air humidity ratios (X_a) at the DCHE_1 inlet and outlet are shown in Fig. 14. Because the DCHE_1 is regenerated (releasing moisture to air) in Mode B, the outlet X_a exceeds that at the inlet. On the contrary, the DCHE_1 dehumidifies the cabin' return air (adsorbing moisture from air) in Mode A, therefore, the outlet X_a is lower than that at the inlet. Furthermore, the outlet X_a at the ending time of Mode A is 2.79g/kg, corresponding to the dew point (DP_{DA}) of -4.2C. Although the surface temperature of the evaporator (T_{sur}) wasn't measured, we don't know whether the anti-fogging relationship of "$DP_{DA}<T_{sur}$" was satisfied. A visual inspection confirmed that neither frost nor drainage was present. Therefore, in the prototype experiments the time of Mode switching was 50 minutes, which exceeds the calculated result of 18 minutes (Fig. 9). The main reason is that the moisture removal rate (M_v) of the DCHE_1 in the prototype is lower compared with the calculation result. Under the same moisture removal capacity, the lower the M_v, the longer the AD time (anti-fogging time). The low M_v in the prototype was mainly caused by the heat capacity change of the DCHE_1 under the switch of adsorption/desorption processes, which is neglected in the simulation.

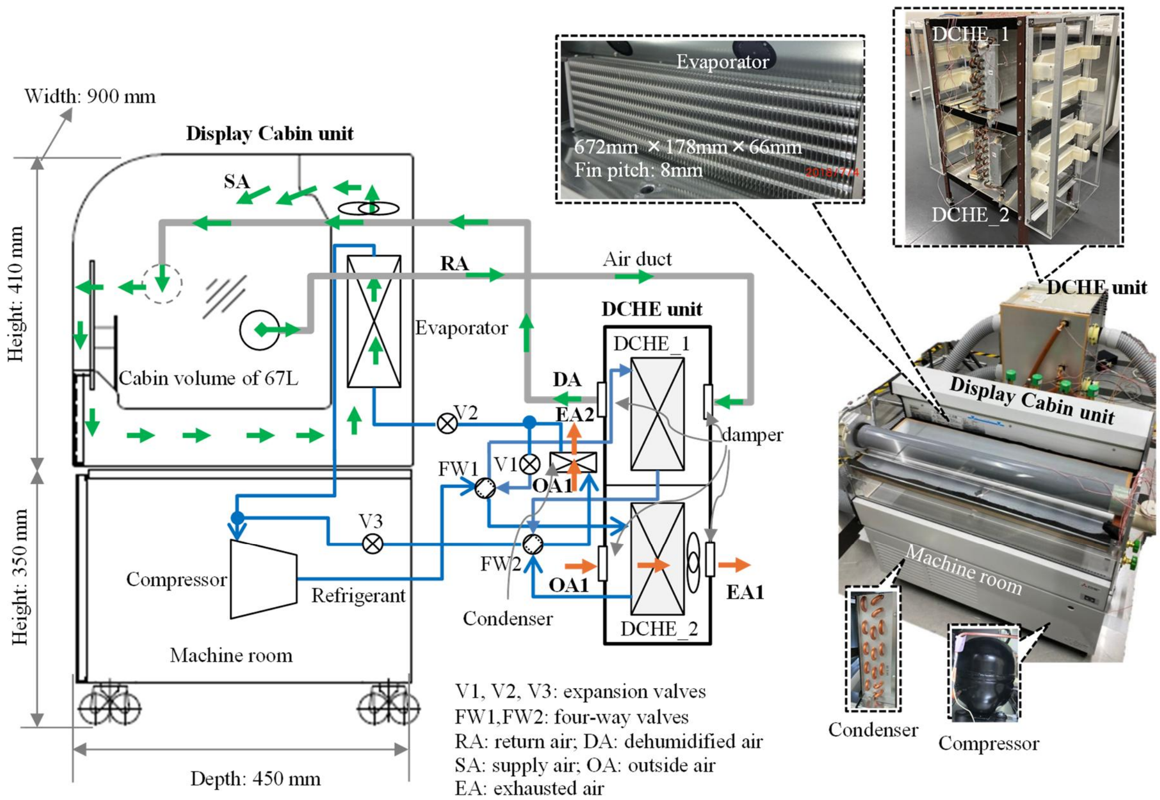

Figure 13 Schematic and photograph of the prototype

The measured results of the cabin temperature (T_{cab}) for both the prototype (frost-free RDC) and a conventional RDC are shown in Fig. 15. Compared to the fluctuating temperature in the conventional RDC, the frost-free RDC can keep an approximately constant T_{cab} of 7°C. It must be noted that for the conventional RDC, T_{cab} rises to 25°C during defrosting process. The proposed frost-free RDC has solved this issue.

The total evaporation heat load of the refrigerant (q_{eva}) and the electric power consumption of the compressor (w_{com}) are shown in Fig. 16. Note that w_{com} is the measurement result, but q_{eva} is obtained based on the measured refrigerant temperature and pressure and the calculated refrigerant mass flow. Here the refrigerant mass flow is calculated based on the specification of the compressor (volume of 12.5cm^3, volume efficiency of 0.7, adiabatic efficiency of 0.52, 60Hz). q_{eva} and w_{om} remain stable except immediately after switching. Furthermore, the average values of total evaporation heat load ($q_{eva,ave}$) and electric power consumption of the compressor ($w_{com,ave}$) in one cycle are calculated and shown in Fig. 17. Compared with the simulation results, $q_{eva,ave}$ of the prototype is 86% higher. Consequently, the prototype's $w_{com,ave}$ exceeds the calculated result. The heat loss of the prototype is the main cause of the increased $q_{eva,ave}$. In the prototype unit, the heat loss by the heat intrusion from the air ducts and refrigerant tubes connecting the display cabin unit with the DCHE unit is significant. Due to some reasons, in this prototype, the DCHE unit was separated from the display unit. However, the ideal configuration of the frost-free RDC involves installing the DCHE unit in the machine room of the display cabin. Accordingly, the heat loss occurring in this prototype could be significantly decreased. Assuming zero heat loss and the adiabatic efficiency of compressor increasing from 0.52 of the prototype to 0.65, namely the value available in the abovementioned simulation, $w_{com,ave}$ could be reduced to 0.18kW. For a conventional RDC product with equivalent cooling capacity, the electric power consumption of the compressor is 0.28kW [24]. Compared to the conventional RDC, the proposed frost-free RDC has the energy saving potential of 36%.

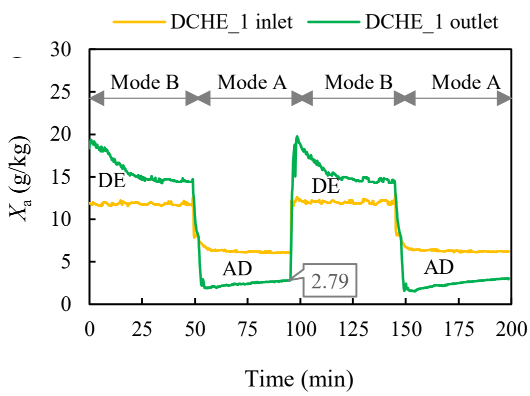

Figure 14 *Xa* at the DCHE_1 inlet and outlet

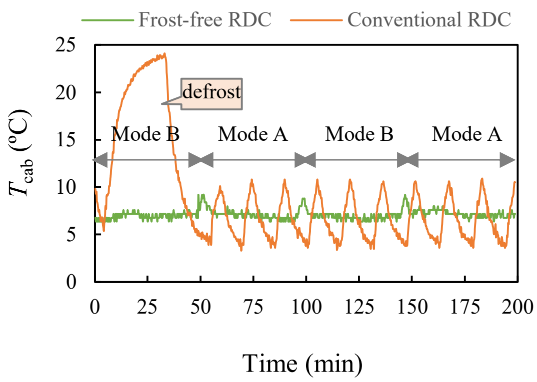

Figure 15 T_{cab} of frost-free RDC and conventional RDC

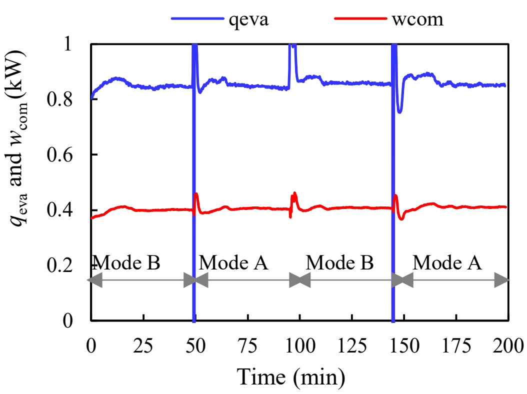

Figure 16 q_{eva} and w_{com}

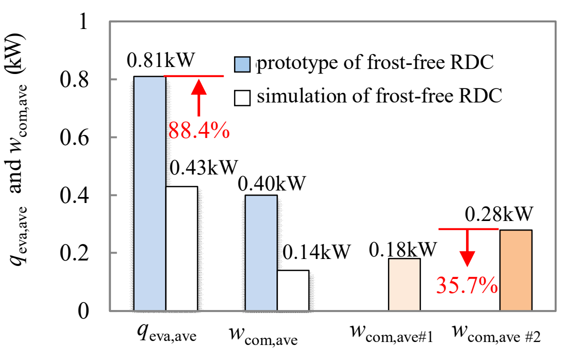

#1: $w_{com,ave}$ of the frost-free RDC when heat loss is 0kW and adiabatic efficiency of compressor is 0.65.
#2: $w_{com,ave}$ of conventional RDC

Figure 17 $q_{eva,ave}$ and $w_{com,ave}$

5. Conclusions

In this study, we proposed a frost-free RDC that mainly comprises a compressor, two desiccant-coated heat exchangers (DCHEs), a low-temperature evaporator and an auxiliary condenser. The return air of the RDC is dehumidified due to one of the DCHEs to prevent the evaporator frosting. Meanwhile, another DCHE works as a condenser, in which the desiccant is regenerated using condensation heat that would otherwise be ejected into the ambient air in conventional RDCs. A theoretical and experimental study is conducted for a forced draft, open-type frost-free RDC, with a cabin volume of 67L and cabin temperature of 2~8°C. Simulation results show that the required air cooling load of the RDC is 0.43kW and the electric power consumption of the compressor is 0.14kW, respectively. A prototype of the frost-free RDC was made and experiments were conducted. The experimental results show that the absence of defrost cycles of the prototype contributes to a stable internal temperature of the cabin. Moreover, the proposed frost-free RDC has an energy saving potential of 35.7% compared to commercial RDCs.

Nomenclature

A - area [m^2]
AD – adsorption
C_p - specific heat at constant pressure [kJ/(kg·K)]
C_w - water content of desiccant [(kg·H_2O)/(kg·desiccant)]
D_{ec} - hydraulic diameter [m]
DCHE - desiccant-coated heat exchanger
DE - desorption
DP - dew point of air [ºC]
RH - relative humidity of air [%]
L - length [m]
h - heat transfer coefficient [kW/(m^2·k)]
i - enthalpy [kJ/kg]
P_r - Prandtl number
m - mass flow rate [kg/s]
M_v - mass-transfer rate [kg/s]
q - heat transfer rate [kW]
q_{st} - latent heat of vaporization of water [kJ/kg]
R_e - Reynolds number
SC - supercooling [ºC]
SH - superheating [ºC]
T - temperature [ºC]
X - humidity ratio of air [g/kg]
δ - thickness [m]
λ - thermal conductivity [kW/(m·K)]
η_{com} - adiabatic efficiency of compressor [-]

Subscripts

a - air
b – brine
cab - cabin
con – condenser
d - desiccant
DA - dehumidified air
eva - evaporator
EA - exhausted air
in - inside
out - outside
OA - outside air
RA - return air
SA - supply air

References

[1] Kondepudi S. N., O'Neal D.L. Effects of different fin configurations on the performance of finned-tube heat exchangers under frosting conditions. ASHRAE Trans. 1990; 96(2), pp. 439-444.
[2] Chen T., Thomas L., Besant R.W. Fan supplied heat exchanger fin performance under frosting conditions. Int. J. Refrig. 2003; 26(1), pp. 140-149.
[3] Silva D. L. d., Hermes C. J. L., Melo C. Experimental study of frost accumulation on fan-supplied tube-fin evaporators. Appl. Therm. Eng. 2011; 31(6-7), 1013-1020.
[4] Huang D., Zhao Liu R. J., Y., et al. Effect of fin types of outdoor fan-supplied finned-tube heat exchanger on periodic frosting and defrosting performance of a residential air-source heat pump. Appl. Therm. Eng. 2014; 69(1-2), pp. 251-260.
[5] Bansal P., Fothergill D., Fernandes R., Thermal analysis of the defrost cycle in a domestic freezer. Int. J. Refrig. 2010; 33. pp. 589-599.
[6] Li Y. M, Huang Y. X., Liu Y. C., et al. Hot gas bypass defrosting with auxiliary heat source in household refrigerators. Appl. Therm. Eng. 2024; 257(C), 124450.
[7] Abdulla M. O. A., Deniz E., Karagöz M., et al. An experimental study on a novel defrosting method for cold room. Appl. Therm. Eng. 2021; 188. 116573.
[8] Melo C., Knabben F. T., Pereira P. V., An experimental study on defrost heaters applied to frost-free household refrigerators. Appl. Therm. Eng. 2013; 51, pp. 239-245.
[9] Wu X. H., Li W. P., Wang W. L., et al. 2017. Experimental investigation of the performance of cool storage shelf for vertical open refrigerated display cabinet. Int. J. Heat Mass Transf. 2017; 110, pp. 789-795.
[10] Lu Y. L., Zhang W. H., Yuan P., et al., Experimental study of heat transfer intensification by using a novel combined shelf in food refrigerated display cabinets (experimental study of a novel cabinets), Appl. Therm. Eng. 2010; 30: pp. 85–91.
[11] Niederer D. H., 1976. Frosting and defrosting effects on coil heat transfer. ASHRAE Transactions 1976; 82 (1): pp. 467-473.
[12] Mei V. C., Gao Z., Tomlinson J. J., Frost-less heat pump. ASHRAE Trans 2002; 108: pp. 452–9.
[13] Demand Defrost Strategies in Supermarket Refrigeration Systems. https://info.ornl.gov/sites/publications/files/pub31296.pdf (accessed November 2025)
[14] Xie G., Bansal, P. K. Analysis of defrosted water evaporation from three water trays in refrigerators. Appl. Therm. Eng. 2000;20: pp. 651-669.
[15] Erten S., öder M., Aktas M., et al. Design and experimental analysis of condensate pan for plug-in refrigerated display cabinets: Improving drying efficiency. Appl. Therm. Eng. 2024;248:23198.
[16] Kondepudi, S., Murali, K., Lorsch, H., Bhalerao, A. Voiding HP evaporator frost by using desiccants. ASME-JSES-JSME Int. Solar Energy Conference 1995; pp. 25-29.
[17] Wang, S. W., Liu, Z. Y. A new method for preventing HP from frosting. Int. J. Refrig. 2005;30: pp. 753-761.
[18] Zhang, L., Fujinawa, T., Saikawa, M. A new method for preventing air-source heat pump water heaters from frosting. Int. J. Refrig. 2012;35: pp. 327-334.
[19] Zhang, L., Fujinawa, T., Saikawa, M. Theoretical study on a frost-free household refrigerator-freezer, Int. J. Refrig. 2016;62: pp. 60-71.
[20] Wang, Z. H., Zheng, Y. X., Wang, F. H., Wang, X. K., Zhang, L., Li, J. C., Chao, H. Experimental analysis on a novel frost-free air-source heat pump water heater system. Appl. Therm. Eng. 2014;70: pp. 808-816.
[21] Desiccant materials. https://www.exlan.co.jp/en/products/desiccant/ (accessed June 2025).
[22] Sushita, Y. and Fujiyi, M. Compact heat exchanger. 1st, The nikkan kogyo Shimbun, LTD. 1992. (in Japanese).
[23] The Japan Society of Mechanical Engineers, Heat transfer. 1st, Maruzen. 2010.
[24] Specifications of refrigerated showcases for daily necessities, dairy products, beverages, and prepared foods:SP-HS362ARC.
https://www.mitsubishielectric.co.jp/ldg/wink/ssl/displayProduct.do?ccd=20301913&pid=208125 (Accessed June 2025).